Congreso de Métodos Numéricos en Ingeniería 2009
Barcelona, 29 junio al 2 de julio 2009


# MODELLING OF BOND BETWEEN GALVANIZED STEEL REBARS AND CONCRETE

**J. Sena-Cruz[1]*, V.M.C.F. Cunha[1], A. Camões[1], J.A.O. Barros[1] and P. Cruz[2]**

1: Departamento de Engenharia Civil
Universidade do Minho
4800-058 Guimarães, Portugal
e-mail: {jsena, vcunha, aires, barros}@civil.uminho.pt,
web: http://civil.uminho.pt/composites/

2: Departamento Autónomo de Arquitectura
Universidade do Minho
4800-058 Guimarães, Portugal
e-mail: pcruz@civil.uminho.pt

**Keywords:** Pullout, local bond, galvanized rebar, epoxy coating, analytical model.

**Abstract**. *In reinforced concrete structures, it is extremely difficult to ensure that steel bars will be not subject, either in a lower or higher extent, to the corrosion effect. The application of hot dip galvanized rebar is an economic and effective way of protecting reinforced concrete against corrosion. This protective technique has an influence, which should not be disregarded, on the performance of the rebar's coating, its behaviour and, fundamentally, the bond between concrete and galvanized rebar. With the aim of studying the bond behaviour between galvanized steel rebar and concrete, an experimental program was carried out by means of direct pullout tests. To predict the full pullout response, an analytical cohesive interface model was developed to obtain the bond stress-slip relationship. To account for the interfacial bond, a nonlinear bond stress-slip law was used. In the present work the numerical method and mathematical tools are detailed and its performance is assessed. Hence, the parameters that define the local bond stress slip relationship are obtained by a fitting procedure between the simulated pullout curve and the experimental one. Finally, the obtained local bond law relationship is compared to the one proposed by the CEB-FIP Model Code.*

## 1. INTRODUCTION

In reinforced concrete structures, it is extremely difficult to ensure that steel bars will be not subject, either in a lower or higher extent, to the corrosion effect. Therefore, to accomplish a long life design of reinforced concrete structures, it should be adopted

mitigating measures for preventing corrosion during the design phase. Within this scope, the effects related to the corrosion of steel rebars should be carefully accounted and estimated, such as: rebar cover thickness; concrete quality; inclusion (or not) of adjuvant inhibitors of corrosion; utilization of rebars of enhanced resistance to corrosion instead of common steel bars. Unfortunately corrosion on rebars may appear, even though adequate measures have been taken, such as: adequate rebar cover thickness; concrete of low permeability; addition of adjuvant inhibitor of corrosion. In fact, it should be remarked that reinforced concrete is prone to cracking, which will promote the penetration of aggressive agents into concrete and thus the contact with reinforcement.

In this context, with the purpose of making the non-alloy steel rebars of reinforced concrete elements more resistant to corrosion, they can be coated with a product which would prevent the direct contact of steel with chlorides, carbon dioxide, moisture and oxygen. Another possibility can be to fully cut off the use of non-alloy steel rebars, thus replacing them by other rebars more resistant to corrosion, such as, stainless steel or other non-metallic materials (fiber reinforced polymer bars). When comparing the latter solutions for preventing corrosion (coating vs. materials resistant to corrosion), from the economic point of view, the first one is, at first sight, more attractive. However, non-alloy rebars with coating (e.g. epoxy, zinc) should conveniently stand up against eventual damage during transportation, packaging and placement operations. The application of hot dip galvanized rebars is an economic and effective way of protecting reinforced concrete against corrosion. This solution is supported in experimental tests and real cases. Galvanizing the steel bars can delay the corrosion initiation of reinforcement and reduce the risk of the concrete structures physical damage due to delamination, cracking and spalling.

In spite of all the aforementioned advantages of galvanized rebars in terms of durability, the effects of the coating on the bond between galvanized rebars and concrete should be assessed, since they can compromise the applicability of these rebars. With the aim of studying the bond behaviour between coated steel bars and concrete, an experimental program was carried out by means of direct pullout tests.

To predict the full pullout response, an analytical cohesive interface model was developed to obtain the bond stress-slip relationship. To account for the interfacial bond, a non-linear bond stress-slip law was used. The mathematical representation of the pullout problem was based on a stress criterion supported on both the problem boundary conditions and a second order differential equation that governs the slip evolution of the rebar. To solve this differential equation an iterative method (Newton-Raphson) and a numerical integration procedure (Runge-Kutta-Nyström) were used. In the present work the numerical method and mathematical tools are detailed and its performance is assessed. Hence, the parameters that define the local bond stress-slip relationship are obtained by a fitting procedure between the simulated pullout curve and the experimental one. Additionally, the local bond law obtained for the galvanized rebars is compared to the one proposed, for conventional steel rebars, by CEB-FIP Model Code 1990 [1].

## 2. EXPERIMENTAL PROGRAM

The main scope of the experimental program was to assess the differences on the pullout behaviour of galvanized steel bars when compared to conventional steel bars. The pullout tests herein presented may be divided into three main groups according to the type of rebars: non-alloy steel bar (without any type of coating), galvanized rebar and galvanized rebar with an epoxy coating. For each of these three main groups, the influence of concrete age (3, 7 and 28 days) on the pullout behaviour was also assessed.

### 2.1. Materials

The concrete composition used in the experimental program was obtained by the Faury method using 350 kg/m$^3$ of cement, 798 kg/m$^3$ of sand and 989.5 kg/m$^3$ of coarse aggregate. The water/cement ratio was 0.5. The average compressive strength for the age of 3, 7 and 28 days was, respectively, 23.8 MPa, 28.7 MPa and 37.8 MPa.
On the other hand, the steel bars used were from the A500 NR class, according to the Portuguese standard E460-2002 [2], with a 20 mm diameter. The average tensile strength for each type of rebar used in the experimental program is included in Table 2..

| Type of rebar | *Effective Diameter* [mm] | *Stress* [MPa] | | *Rupture Strain* [%] |
|---|---|---|---|---|
| | | *Yield* | *Rupture* | |
| Non-alloy steel bar | 20.5 | 567.5 | 689.5 | 13.0 |
| Galvanized | | 525.0 | 634.0 | 16.3 |
| Galvanized + epoxy | | 537.0 | 655.0 | 15.8 |

Table 1. Mechanical properties of the steel bars (average values).

The results from the tensile tests on the distinct rebars show that the galvanization process has reduced the yield and rupture stresses in approximately 7%, and has increased the rupture strain in nearby 25%. As expected, the employment of an epoxy coating over the galvanized rebar surface does not alter significantly the mechanical properties of steel.

### 2.2. Test set-up and specimens

Cubic specimens with an edge of 200 mm were prepared according to the Rilem-RC6 recommendations [3]. The rebar which will be pulled-out was positioned in the centre of the mould and with two protruding ends (see Fig. 1). Rebar and concrete are only bonded in half length of the cubic specimen, in order to exclude an eventual confinement of the concrete surrounding the rebar due to the stress distribution on the specimen surface in contact with testing rig (see Fig. 2). During the specimen casting, concrete was placed in the moulds in the perpendicular direction of the rebars, so-called “rebars casted in the horizontal”.

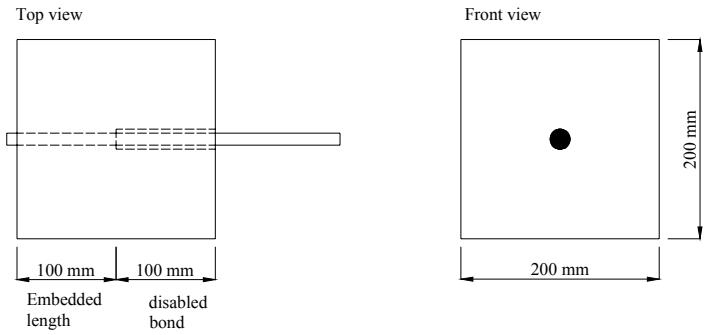


Figure 1. Dimensions of the specimens used in the pullou tests.

In Fig. 2 is depicted the pullout test set-up. The slip of the rebar was measured on the free-end, i.e. opposite to the loaded-end, which was fastened to a grip and where the pullout load was applied. The displacement transducer had a measuring stroke of ±10 mm and an accuracy of ±0.01 mm.

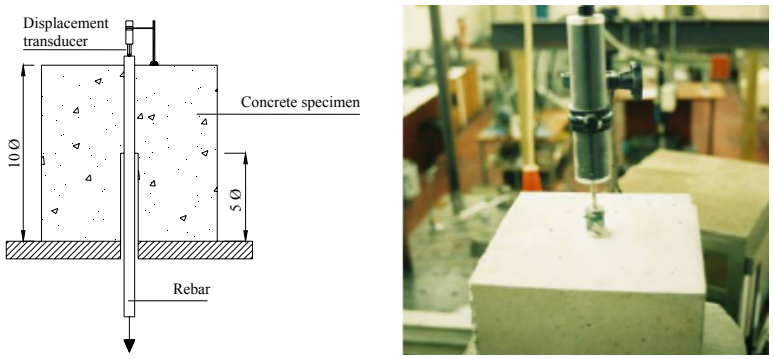


Figure 2. Pullout test set-up.

## 2.3. Test results

In Fig. 3 are represented the experimental pullout load *vs*. free-end slip relationships for each tested specimen. From the analysis of Fig. 3(a) can be ascertained that, in general, the galvanized and non-alloy rebars at an age of 3 days showed similar pullout behaviour. In fact, for the galvanized rebars, the average maximum pullout load was just 2% lower than in the non-alloy rebars. On the other hand, the galvanized rebars coated with epoxy had a significantly lower average maximum pullout load (nearby 40%). Regarding the pullout tests performed at the age of 7 days, the average maximum pullout load for the galvanized rebars was approximately 25% lower than for the non-alloy rebars, whereas for the galvanized rebars coated with epoxy was nearby 55% lower. Finally, for pullout tests at the age of 28 days similar trends were observed. The galvanized rebars, without and with

epoxy coating, had an average maximum pullout load, respectively, 15% and 42% lower than the non-alloy rebars.

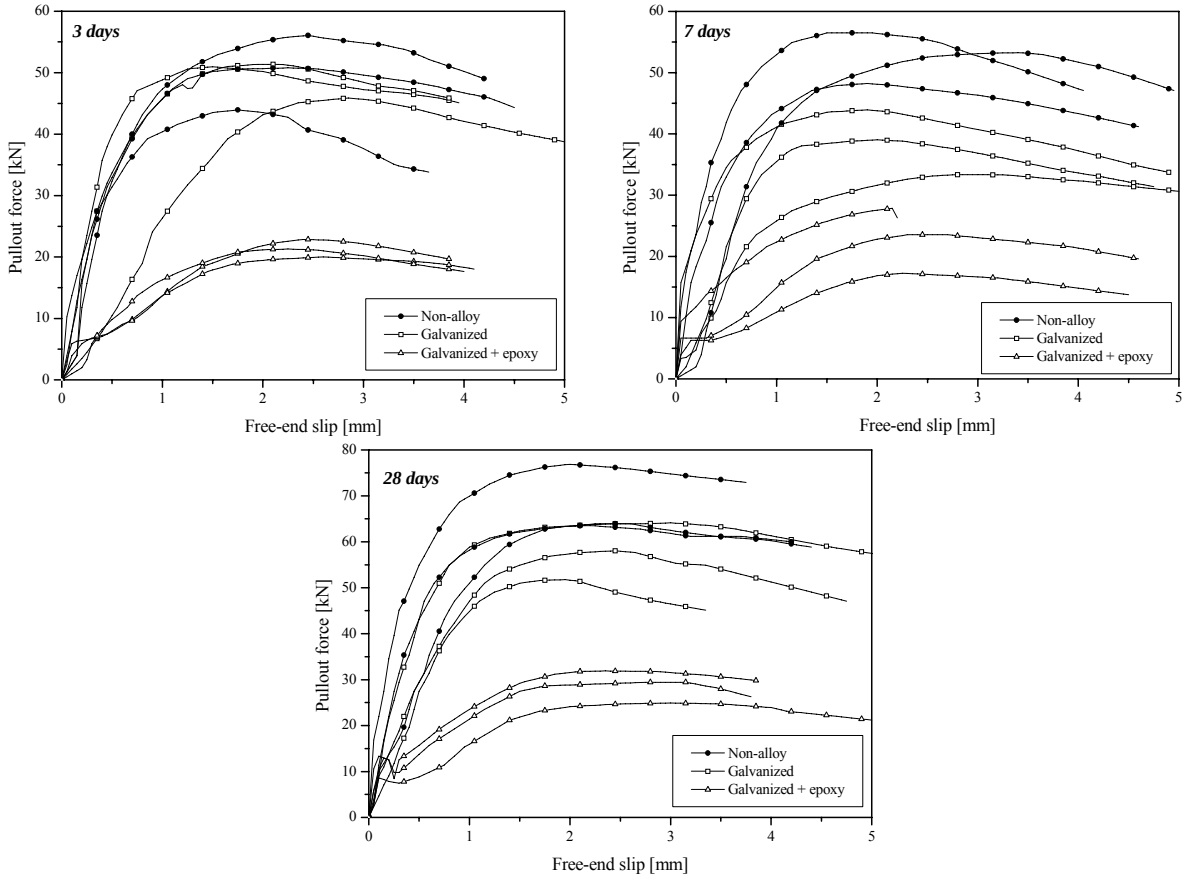


Figure 3. Experimental pullout load vs. free-end slip curves.

## 3. ANALYTICAL MODEL FOR BOND-SLIP LAW

The pullout problem is often represented by a second order differential equation, established in terms of forces [4-6]. However, in the present model the differential equation was derived in terms of slip [7-9] due to the following two main reasons: the displacements of the concrete volume at the interface between concrete and rebar were neglected; bar-concrete slips were obtained from the experimental tests, therefore the bond-slip problem needs to be formulated in terms of the free-end slip.

### 3.1. Local bond-slip

The equilibrium of the free body with an infinitesimal length *dx* of a rebar bonded to a

concrete matrix can be given by:

$$\sigma_f \cdot A_f + \tau \cdot P_f \cdot dx = \left(\sigma_f + d\sigma_f\right) \cdot A_f \tag{1}$$

where $\tau = \tau(s(x))$ is the local bond shear stress acting on the contact surface between rebar and concrete, and $s$ is the slip, i.e. the relative displacement between the rebar and the concrete. Finally, $\sigma_f$, $A_f$ and $P_f$ are the normal stress, cross-section area and perimeter of the rebar, respectively.

Assuming that the rebar has a linear elastic constitutive law in the longitudinal direction ($d\sigma_f = E_f \cdot d\varepsilon_f$) and neglecting the concrete deformability in the slip determination, after simplification of Eq. 1, the second order differential equation that governs the local bond phenomena of the rebar matrix interface is given by:

$$\frac{d^2 s}{dx^2} = \frac{P_f}{E_f A_f} \cdot \tau(x) \tag{2}$$

Remark that, the contribution of the concrete deformability in the slip assessment may be neglected, since the rebar is subjected to large inelastic deformations. Several authors have neglected this component, on the evaluation of the bond-slip relationship of reinforcing bars [7], FRP reinforcement [8,9] and discrete steel fibers [10].

### 3.2. Pullout load-slip relationship

Consider a steel rebar embedded on a concrete matrix over a bond length $L_b$, where $N$ is the generic applied pullout force, and $s_f$ and $s_l$ are, respectively, the free and loaded end slips starting at the free end of the rebar (see Fig. 4). When the rebar is slipping due to an applied pullout force, $\bar{N}$, the following functions can be evaluated along the rebar bond length: slip along the rebar, $s(x)$; bond shear stress along the embedded length, $\tau(x)$; rebar strain, $\varepsilon_f$; and the axial force, $N(x)$.

In Fig. 4 the slip diagram along the rebar, $s(x)$, can be regarded as the sum of two components. A constant component, $s_f$, which produces a rigid body displacement of the rebar, whereas the $s_d(x)$ component results from the deformation of the rebar. Moreover, for any point $x$ of the rebar embedded length, just the $s_d(x)$ component will result in a rebar length change, and, therefore, contributing to the rebar deformation energy. Likewise, the axial force along the rebar, $N(x)$, will contribute to the rebar deformation energy. Therefore, the rebar deformation at a point $x$ is obtained from $\varepsilon_f(x) = N(x)/(E_f A_f)$.

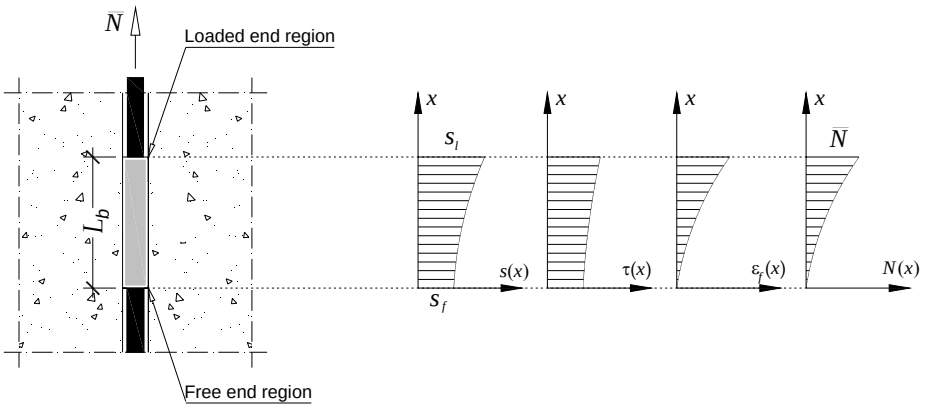


Figure 4. Entities in the analytical model.

Considering a generic rebar cross-section at the interval $0 \le x \le L_b$, and that the rebar lateral surface over embedded length $\bar{x}$ is $\Omega = P_f \cdot \bar{x}$, the work performed by external forces acting on the range $0 \le x \le L_b$ is:

$$W_{ext} = \int_{\Omega} \left( \int_{s_f}^{s(x)} \tau(s) \cdot ds \right) d\Omega = P_f \int_0^{\bar{x}} \left( \int_{s_f}^{s(x)} \tau(s) \cdot ds \right) dx \tag{3}$$

On the other hand, remarking $V_f = A_f \cdot \bar{x}$ as the rebar volume over the embedded length, the elastic energy of the rebar is:

$$\begin{aligned} W_{\text{int}} &= \int_{V_f} \left( \int_0^{\varepsilon(x)} \sigma_f(\varepsilon_f) \cdot ds \right) dV_f = A_f \int_0^{\bar{x}} \left( \int_0^{\varepsilon(x)} E_f \varepsilon_f \cdot d\varepsilon \right) dx \\ &= \frac{A_f}{2E_f} \int_0^{\bar{x}} \sigma_f^2(x) \cdot dx \end{aligned} \tag{4}$$

From Eq. 3 and 4 is obtained:

$$\int_0^{\bar{x}} \left( P_f \int_{s_f}^{s(x)} \tau(s) \cdot ds - \frac{A_f}{2E_f} \sigma_f^2(x) \right) dx = 0 \tag{5}$$

Since Eq. 5 must be satisfied for each value of $0 \le x \le L_b$, the latter may be rewritten as:

$$P_f \int_{s_f}^{s(x)} \tau(s) \cdot ds - \frac{A_f}{2E_f} \sigma_f^2(x) = 0 \tag{6}$$

At $x=L_b$, Eq. 5 becomes:

$$P_f \int_{s_f}^{s(x=L_b)} \tau(s) \cdot ds - \frac{N^2}{2E_f A_f} = 0 \tag{7}$$

$$N = \sqrt{2E_f \cdot A_f \cdot P_f \cdot \int_{s_f}^{s(x=\tilde{L}_b)} \tau(s) \cdot ds} \tag{8}$$

### 3.3. Numerical procedure

The adopted method is supported on the work developed by [8,9]. In order to improve the performance of the method and to adapt it to the specificities of the present study, some modifications were performed. In this section, the implemented algorithm is described in detail.

Considering the entities described in Fig. 3, the boundary conditions at the free and loaded ends are indicated in Eq. 9. In the present method, numerical and experimental entities are simultaneously used; hence the experimental one was distinguished by an overline, i.e. $\overline{N}^i$ represents for the pullout force experimentally measured in the *i-th* experimental scan read-out.

$$x = 0 \rightarrow \begin{cases} s(0) = s_f \\ N(0) = 0 \\ \varepsilon_f(0) = 0 \end{cases} \qquad x = L_b \rightarrow \begin{cases} s(L_b) = s_l \\ N(L_b) = \overline{N} \\ \varepsilon_f(L_b) = N\left(L_b\right) / \left(E_f A_f\right) \end{cases} \tag{9}$$

The rebar pullout tests provide data in terms of pullout force, $\overline{N}$, and free-end slip, $\overline{s}_f$, for several scan read-outs, being $\overline{s}_f^i$ and $\overline{N}^i$ the values of the *i-th* scan read-out. Regarding these experimental results, the set of unknown parameters of a given local bond relationship is desired to be found in order to fit the differential Eq. 2 as accurately as possible.

A computational code was developed and implemented, supported on the algorithm described in Fig. 5. The second order differential Eq. 2 included in the algorithm is solved by the Runge-Kutta-Nyström (RKN) method. Further details of the latter method can be found elsewhere [11]. The algorithm is built up from the following main steps:

1- The $\tau$-$s$ relationship is defined attributing values to the unknown parameters. The error, $\overline{e}$, defined as the area between the experimental and analytical pullout force-slip curves, is initialized;
2- The numerical loaded end slip is calculated at the onset of the free end slip, $\tilde{s}_l$, (see Module A in Fig. 6);
3- For the experimental *i-th* experimental scan reading, the loaded end slip, $\tilde{s}_f^i$, and the pullout force, $\overline{N}$ are read;
4- Taking the free-end slip, $\overline{s}_f^i$, and using Eq. 2, the numerical pullout force at the loaded end, $N^i(\overline{s}_f^i)$, is evaluated (see Module B in Fig. 6).
5- The error associated with $\overline{N}(s_f^i)$ is calculated. This error is the area between the

experimental ( $A^i_{\exp,f}$ ) and numerical ( $A^i_{num,f}$ ) curves. The points $\left(\overline{s}_f^{i-1}, N^{i-1}(\overline{s}_f^{i-1})\right)$ and $\left(\overline{s}_f^{i}, N^{i}(\overline{s}_f^{i})\right)$ are used to define the numerical curve, whereas the experimental curve is represented by the points $\left(\overline{s}_f^{i-1}, \overline{N}^{i-1}\right)$ and $\left(\overline{s}_f^{i}, \overline{N}^{i}\right)$;

6- The error is updated.

7- Taking the loaded end slip, $\overline{s}_l^i$, and using Eq. 2, the pullout force at the loaded end, $N^i(\overline{s}_l^i)$, is evaluated. In this case the following two loaded end slip conditions must be considered:

   i) if $\overline{s}_l^i < \tilde{s}_l$, the determination of $N^i(\overline{s}_l^i)$ must take into account that the effective bond length is smaller than $L_b$ (see Module C in Fig. 6);

   ii) if $\overline{s}_l^i > \tilde{s}_l$, the evaluation of $N^i(\overline{s}_l^i)$ is based on Module D (see Fig. 6);

8- The error associated with $N^i(\overline{s}_l^i)$ is calculated. This error is the area between the experimental $\left(A^i_{\exp,l}\right)$ and numerical $\left(A^i_{num,l}\right)$ curves. The points $\left(\overline{s}_l^{i-1}, N^{i-1}(\overline{s}_l^{i-1})\right)$ and $\left(\overline{s}_l^{i}, N^{i}(\overline{s}_l^{i})\right)$ are used to define the numerical curve, whereas the experimental curve is represented by the points $\left(\overline{s}_l^{i-1}, \overline{N}^{i-1}\right)$ and $\left(\overline{s}_l^{i}, \overline{N}^{i}\right)$;

9- The error is updated.

In *Modules C* and *D* the Newton-Raphson method is used. When the Newton-Raphson method fails, the bisection method is used as an alternative.

The determination of the unknown parameters defining the bond stress-slip relationship, $\tau$-$s$, was performed by a back-analysis, i.e. determining the $\tau$-$s$ relationship in such a way that the difference between the numerical and experimental pullout force-slip curves provides a minimum error, e. Additionally, two restriction conditions were added in order to assure similar values between the numerical and experimental peak pullout force and its corresponding slip (with a tolerance smaller than 2%).

The back-analysis was performed by the exhaustive search method (brute force method), based on several parameters sets ascertained by a predefined range and step for each parameter of the corresponding set.

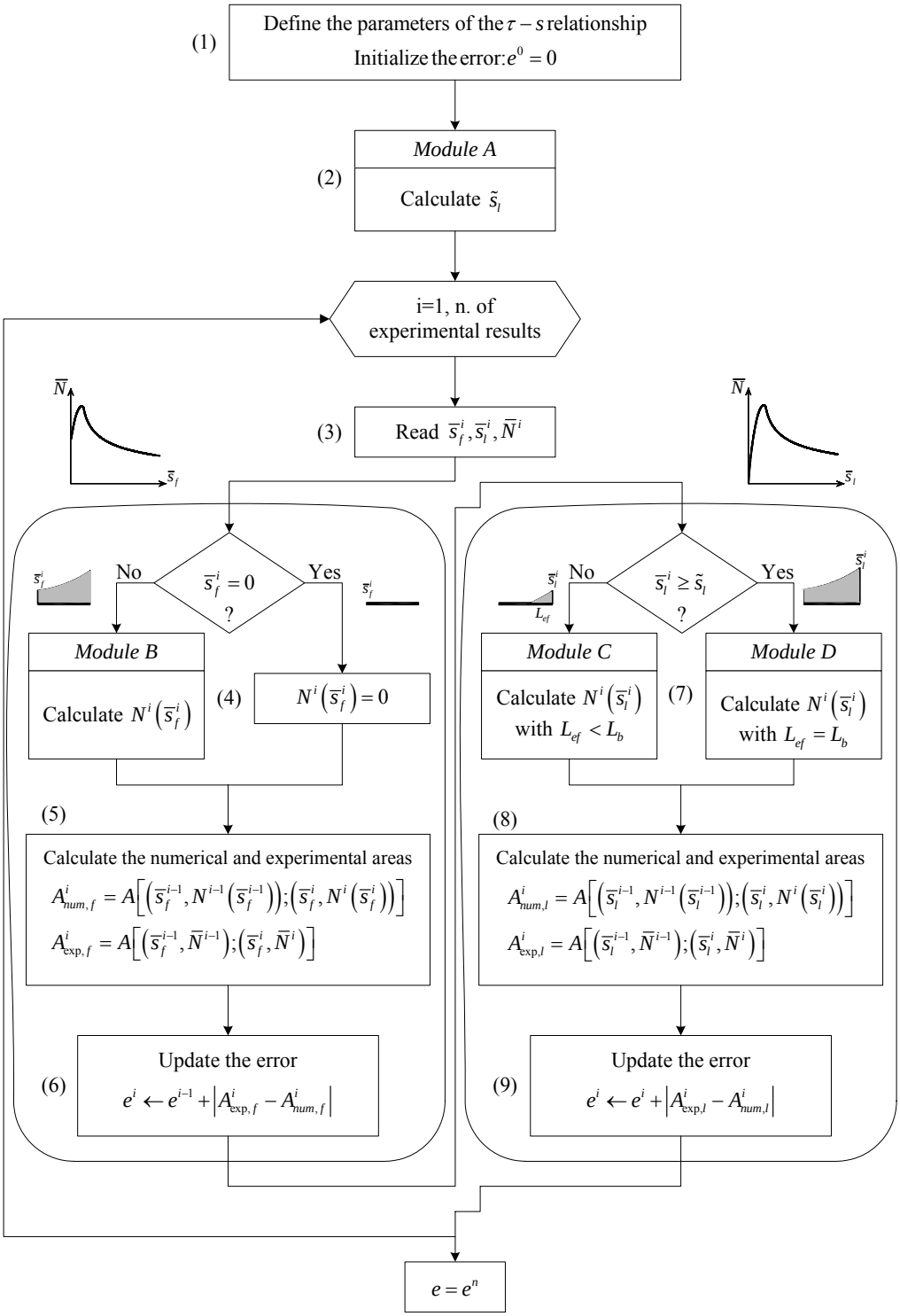


Figure 5. Algorithm to obtain the local bond-stress slip relationship.

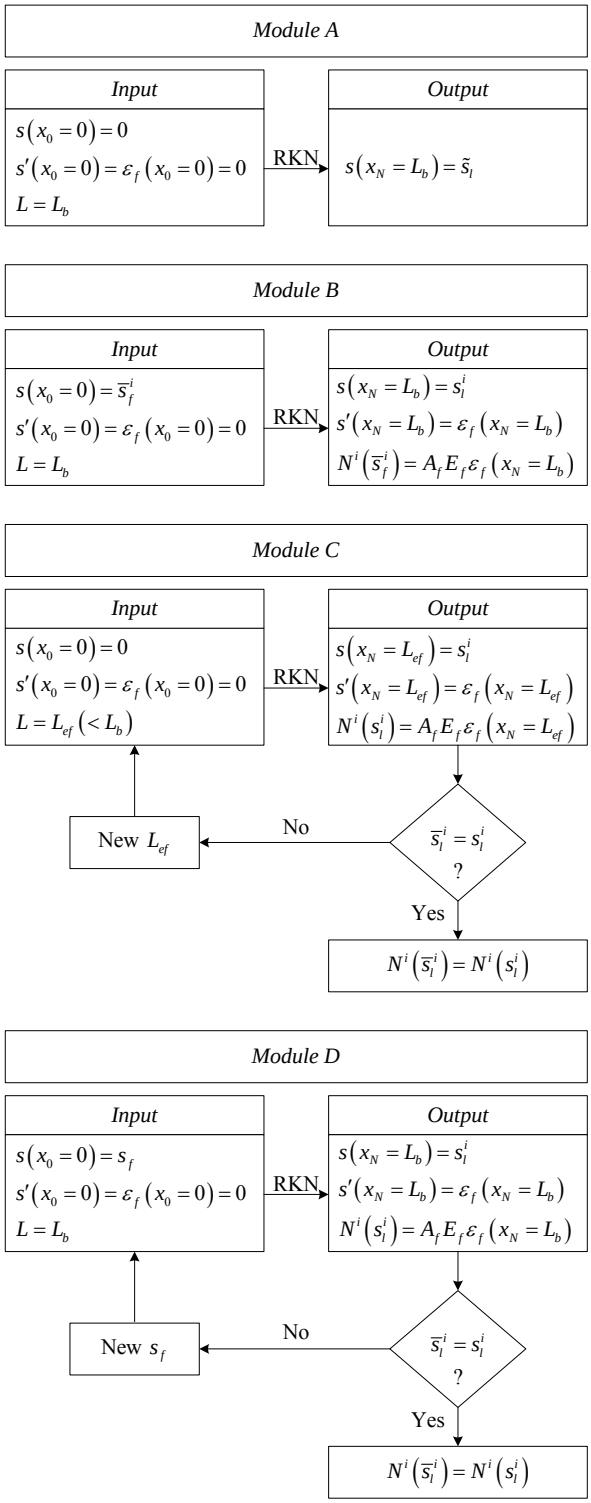


Figure 6. Modules A, B, C and D of the algorithm shown in Fig. 5.

## 4. NUMERICAL SIMULATION

### 4.1. Based on CEB-FIP Model Code-90 relationships

In Fig. 7 is depicted the bond stress-slip relationship proposed by [1]. On the other hand, the parameters of the latter relationship for ribbed reinforcing steel and confined concrete are given in Table 2.

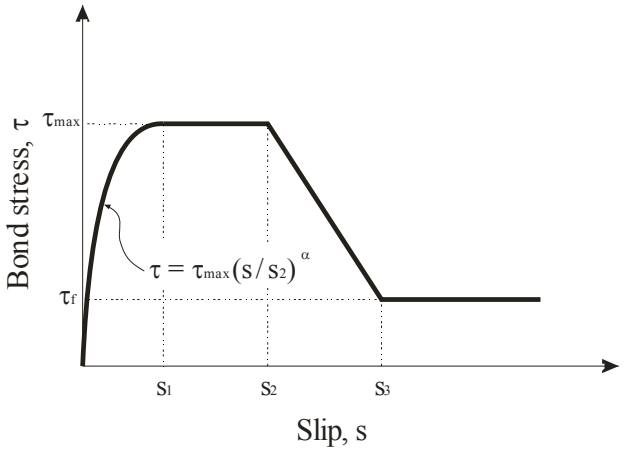


Figure 7. Local bond stress-slip law according to [1].

| *Bond conditions* | $\tau_{max}$ | $\tau_f$ | $\alpha$ [-] | $s_1$ [mm] | $s_2$ [mm] | $s_3$ [mm] |
|---|---|---|---|---|---|---|
| Good | $2.5\sqrt{f_{cm}}$ | $0.4\cdot\tau_{max}$ | 0.4 | 1 | 3 | Clear rib spacing of rebar |
| All other | $1.25\sqrt{f_{cm}}$ | $0.4\cdot\tau_{max}$ | 0.4 | 1 | 3 | |

Table 2. Parameters for defining the bond-slip relationship [1].

To simulate the experimental results, the numerical model described in Section 3 was used with the bond stress-slip law shown in Figure 7. For the simulation of the non-alloy rebars was assumed good bond conditions (see Table 2). For the case of galvanized + epoxy steel bars other bond conditions were adopted. Finally, in the simulation of the galvanized rebars, intermediate values between good and other bond conditions in terms of tangential stresses were adopted (i.e. $\tau_{max}$=11.53 MPa and $\tau_f$=4.61 MPa). In Figure 8 the obtained results are depicted. These figures show that using the proposed law by Model Code 1990 with the parameters presented in Table 2 is not suitable to simulate the present experimental results.

### 4.2. Based on inverse analysis

The numerical simulation of the experimental pullout curves using the bond-slip law suggested by the Model Code 1990 was not accurate, especially, for the galvanized rebars and galvanized + epoxy rebars. Indeed, for the latter, the maximum pullout force was clearly overestimated. This discloses that the bond strength for these types of rebars is smaller than for conventional rebars. Moreover, the first stage of the pullout response was not well modeled. Therefore, new parameters for the definition of the local bond stress law ($\tau_{max}$, $s_1$, $\alpha$) presented in the prior section were obtained by inverse analysis.
In Figure 8 are depicted the numerical curves obtained with the proposed model by inverse analysis. Additionally, in Table 3 are included the local bond law parameters for the corresponding numerical simulation. The numerical simulation by inverse analysis has fitted the experimental data with good agreement.

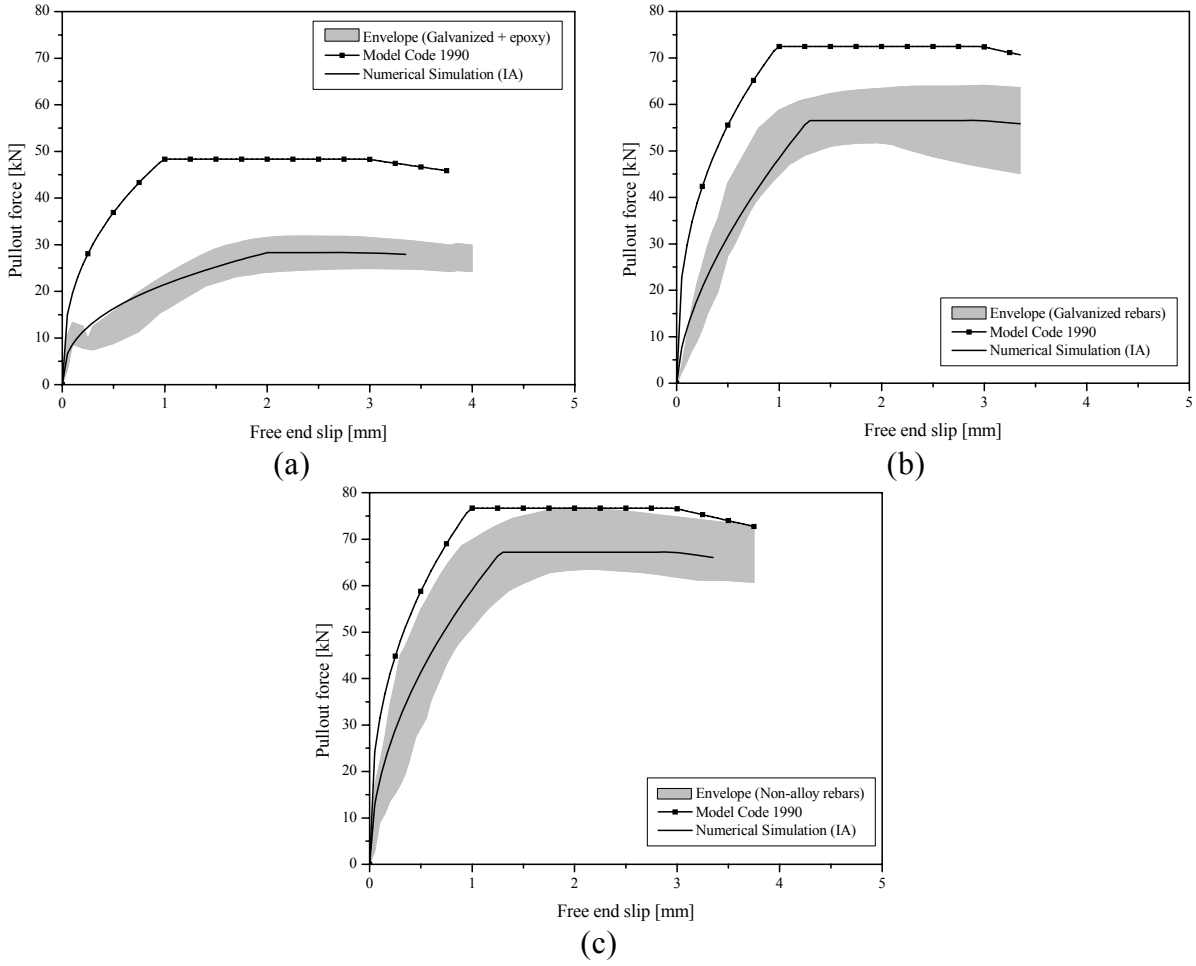


Figure 8. Numerical simulation of the experimental pullout curves at 28 days for: (a) Galvanized + expoy rebars, (b) Galvanized rebars and (c) Non-alloy rebars.

| *Rebar* | $\tau_{max}$ | $s_1$ [mm] | $\alpha$ [-] | Error [%] |
|---|---|---|---|---|
| Galvanized + epoxy | $0.73\sqrt{f_{cm}}$ | 2.00 | 0.40 | 3.9 |
| Galvanized | $1.46\sqrt{f_{cm}}$ | 1.30 | 0.62 | 2.5 |
| Non-alloy | $1.75\sqrt{f_{cm}}$ | 1.30 | 0.52 | 1.8 |

Table 3. Parameters of the bond-slip relationship obtained by inverse analysis.

## 5. CONCLUSIONS

With the aim of studying the bond behaviour between galvanized and galvanized-epoxy coated steel bars and concrete, an experimental program was carried out by means of direct pullout tests.

To predict the complete pullout response, an analytical cohesive interface model was developed to obtain the bond stress-slip relationship. To account for the interfacial bond, a non-linear bond stress-slip law should be used.

In the present work, the local bond law proposed by CEB-FIP Model Code-90 was used. This law can accurately simulate the experimental results just by fitting some of its parameters.

## REFERENCES

[1] CEB-FIP, *CEB-FIP Model Code 1990 – Design Code*, Thomas Telford, Lausanne, Switzerland, (1993).

[2] LNEC E460-2002, *Varões de Aço A500 NR de ductilidade especial para armaduras de betão armado – Características, ensaios e marcação*, Laboratório Nacional de Engenharia Civil, Lisboa, (2002).

[3] RILEM-CEB-FIP, *Recomendations on reinforcement steel for reinforced concrete. Revised edition of: RC6 Bond test for reinforcement steel (2) Pull-out test*, Comité Euro International du Betón, N. 61, Paris, April, (1982).

[4] A. E. Naaman, G. G. Namur, J. M. Alwan, H. S. Najm. "Fiber pullout and bond slip I: Analytical study", *Journal of Structural Engineering ASCE*, Vol. **117**(9), p.p. 2769-2790 (1990).

[5] B. Banholzer, W. Brameshuber, W. Jung. "Analytical simulation of pull-out tests – the direct problem", *Cement & Concrete Composites*, Vol. **27**, p.p. 93-101 (2005).

[6] Sujivorakul, C., Waas, A. M. and Naaman, A. "Pullout response of a smooth fiber with an end anchorage.", *Journal of Engineering Mechanics*, Vol. **126**(9), p.p. 986-993, (2000).

[7] Russo, G., Zingone, G. and Romano, F. "Analytical solution for bond-slip of reinforcing bars in R.C. joints", *Journal of Structural Engineering ASCE*,

Vol. **116**(2), p.p. 336-355, (1990).

[8] Focacci, F., Nanni, A. and Bakis, C. "Local bond-slip relationship for FRP reinforcement in concrete." *Journal of Composites for Construction ASCE*, Vol. **4**(1), p.p. 24-31, (2000).

[9] Sena-Cruz, J.M., Barros, J.A.O. "Modeling of bond between near-surface mounted CFRP laminate strips and concrete", *Computers and Structures Journal*, Vol. **82**, p.p. 1513-1521, (2004).

[10] Cunha, V.M.C.F., Barros, J.A.O., Sena-Cruz, J.M., *Analytical model for bond-slip of hooked-end steel fibres*, Torres Marques et.al eds *CCC2008 – Chalenges for Civil Construction*, FEUP, Porto (2008).

[11] Kreyszig, E., *Advanced Engineering mathematics*, John Wiley & Sons, Inc, (1993).